



2 **Comparative studies of thermal and mechanical properties**
3 **of macrocyclic versus linear polylactide**

4 Elodie Louisy^{1,2} · Gaëlle Fontaine¹ · Valérie Gaucher¹ · Fanny Bonnet¹ ·
5 Grégory Stoclet¹

6 Received: 22 January 2020 / Revised: 5 May 2020 / Accepted: 27 June 2020
7 © Springer-Verlag GmbH Germany, part of Springer Nature 2020

8 **Abstract**

9 This paper reports the study of the influence of the macrocyclic or linear topology
10 of polylactide (PLA) on its resulting thermal and mechanical properties, when dis-
11 playing identical molar masses. Even if both macrocyclic and linear PLAs crystal-
12 lize in the same α phase, the results of the calorimetric study and of the tensile tests
13 show some differences which are directly related to the topology of the polymer.
14 The glass transition temperature of macrocyclic PLA was found to be slightly higher
15 than that of the linear one (56 vs 53 °C) while its melting temperature is lower (165
16 vs 171 °C). Moreover, the crystallization rate of the macrocyclic PLA is slower
17 than that of the linear PLA. Regarding the tensile tests, it has been observed that
18 the macrocyclic PLA displays an earlier strain-hardening than the linear one when
19 stretched in the rubbery state. These differences were attributed to the fact that the
20 macrocyclic topology involves a more constrained entangled network than its linear
21 analogous and/or that the disentanglement kinetics is faster in linear PLA than in
22 macrocyclic PLA.

23 **Keywords** Macrocyclic polylactide · Linear polylactide · Thermal properties ·
24 Mechanical properties · Macromolecular network

A1 **Electronic supplementary material** The online version of this article (<https://doi.org/10.1007/s00289-020-03290-5>) contains supplementary material, which is available to authorized users.

A3 ✉ Fanny Bonnet
A4 fanny.bonnet@univ-lille.fr

A5 ✉ Grégory Stoclet
A6 gregory.stoclet@univ-lille.fr

A7 ¹ Univ. Lille, CNRS, INRAE, Centrale Lille, UMR 8207 - UMET - Unité Matériaux Et
A8 Transformations, 59000 Lille, France

A9 ² Univ. Lille, CNRS, Centrale Lille, Univ Artois, UMR 8181 - UCCS - Unité de Catalyse Et de
A10 Chimie du Solide, 59000 Lille, France

25 Introduction

26 Despite the numerous advantages of synthetic petrochemical-based polymers, two
 27 major drawbacks are still remaining: the use of non-renewable resources to pro-
 28 duce them along with their end-life. In this context, developing petroleum-free
 29 and biodegradable materials is of high interest. Thus, polylactide (PLA) is par-
 30 ticularly relevant as it derives from 100% renewable natural resources, such as
 31 corn or beets, and it is also biocompatible and biodegradable [1–3]. These latter
 32 properties have contributed to increase its use in various applications, and par-
 33 ticularly in medical fields [4]. Furthermore, even if PLA finds numerous short
 34 life-time applications, it tends to be considered for longer life-time purposes as
 35 blends [5, 6] or composites [7]. PLA can be synthesized by direct condensation
 36 of lactic acid [8] or by ring-opening polymerization (ROP) of lactide [9, 10].
 37 Among ROP methods, coordination-insertion ROP of lactides (LA) monitored by
 38 metal-based catalysts is a powerful and versatile technique, allowing access to
 39 well-defined high molar mass polymers [8–10].

40 Isotactic polylactides can be prepared directly by the ROP of optically pure
 41 L-LA or D-LA, whereas racemic lactide (*rac*-LA) or meso-lactide (*meso*-LA)
 42 will usually give rise to atactic polymers, unless specific catalysts are used, in this
 43 case heterotactic or isotactic PLA will be obtained [10]. Isotactic poly(L-LA) is a
 44 highly crystalline material with a melting temperature (T_m) of 170 °C which dis-
 45 plays good mechanical properties [1] and degrades rather slowly, whereas atactic
 46 poly(*rac*-LA) is amorphous and subject to faster degradation [11].

47 In a previous study, we have reported the synthesis of high molar mass macro-
 48 cyclic polylactide by polymerization of L-lactide under reactive extrusion condi-
 49 tions with lanthanide trisborohydrides complexes, $\text{Ln}(\text{BH}_4)_3(\text{THF})_3$ ($\text{Ln} = \text{La}, \text{Sm}$
 50 or Nd), as the catalysts [12]. Various investigations have shown that the cyclic
 51 topology of a polymer leads to differences in material properties compared to the
 52 linear one, such as increased glass transition temperatures (T_g), smaller hydrody-
 53 namic volumes and lower intrinsic viscosities [13–15]. Moreover, both the mass
 54 and hydrodynamic volumes are substantially reduced compared to linear counter-
 55 parts, providing a retarded hydrolytic degradation profile [16, 17]. As polylactide
 56 exhibits both biodegradability and biocompatibility, this cyclic topology may pro-
 57 vide advantages for a range of biomedical applications, such as novel drug deliv-
 58 ery vectors [16, 17] or supramolecular hosts [18].

59 In a recent paper, Zaldua et al. studied the influence of the topology on the
 60 crystallization behavior of PLA [19]. Besides, they found that even if the topology
 61 has no effect on the crystal structure, this parameter clearly infers on nucleation
 62 and consequently crystallization kinetics. Particularly, cyclic PLA chains nucleate
 63 much faster than linear ones while no significant effect is observed regarding the
 64 growth rate. They explain these differences by both kinetics and thermodynam-
 65 ics effects, and especially by a faster diffusion capacity of the cyclic chains and
 66 a lower density of entanglements in cyclic PLA. However, in their study, authors
 67 studied linear and cyclic PLA displaying molar masses around 10,000 g/mol, that
 68 is to say close to the mass between entanglements (M_e) of PLA which is known

to be around 6000–9000 g/mol [20–22] and thus below the critical molar mass (M_c) which is considered as the critical molar mass values needed to form entanglements. Consequently, it can be assumed that such materials are un-entangled ones and have a brittle behavior and limited mechanical properties limiting their application fields. In addition, due to the synthesis method they used, *i.e.*, the ring closure, some macrocycles and/or linear chains are present into their cyclic PLA, which can infer on the behavior observed.

In the present work, we synthesized two batches of purely linear and macrocyclic polylactides displaying the same molar masses of $\approx 30,000$ g/mol, in order to study the influence of their topology on the resulting thermal and mechanical properties. These investigations were conducted by DSC analysis, tensile tests as well as WAXS analyses.

Material and methods

Reagents

L-lactide (L-LA), supplied by Purac, was conditioned in small sealed bags under vacuum, stored in a glove box ($O_2 = 0$ ppm & $H_2O = 2$ ppm) and used as received (H_2O content, measured by Karl-Fischer analysis, was found inferior to 5 ppm). The sealed bags were open just before mixing L-lactide with the catalyst in the glove box. $La(BH_4)_3(THF)_3$ was synthesized according to the literature procedure [23].

Toluene was supplied by VWR Chemicals (purity $\geq 99.5\%$, Analar Normapur) and purified in a MBRAUN SPS-800 solvent system. Non-anhydrous chloroform was supplied by Verbiess (purity of 99% stabilized with ethanol). Diethyl ether was supplied by Honeywell (contains BHT as inhibitor, purity $\geq 99.8\%$). $CDCl_3$ was supplied by Aldrich (purity of 99.8% of D). THF 99+%, extra pure (stabilized with BHT) was supplied by Acros Organics.

Synthesis of macrocyclic and linear PLA

Macrocyclic PLA was synthesized according to our previously reported procedure [12]. L-lactide (20 g, 0.139 mol) and $La(BH_4)_3(THF)_3$ (55 mg, 1.39×10^{-4} mol) were weighted and mixed together in a glass bottle in a glove box with a manual stirring, before feeding the extruder. The polymerization was performed in a co-rotating twin screw microextruder, from DSM (Geleen, the Netherlands) under nitrogen at a temperature of 130 °C using a residence time of 80 min, and a screw speed of 100 rpm. The conversion of the reaction was determined by 1H NMR analysis of a sample of polymer in $CDCl_3$ and found to be 85%.

In order to purify the obtained macrocyclic PLA, the sample was cryogenically ground and the residual L-lactide was sublimated under vacuum. The cryogrinding was carried out with a Retsch ZM 200. The samples were cryogenically ground at a speed of 10,000 rpm for 30 s. The cryogenically ground polymer was then introduced in a cold finger sublimator immersed in an oil bath heated to

108 90 °C in order to sublime the residual monomer. This treatment allowed us to
 109 isolate macrocyclic PLA with residual monomer content of 3% ($M_n = 29\,490\text{ g mol}^{-1}$, $D = 1.27$). The macrocyclic structure of the obtained PLA was confirmed
 110 by performing MALDI-ToF analysis on our sample (Fig. 1 and S4).
 111

112 *Linear PLA* was synthesized according to a literature procedure [24]. L-lactide
 113 (10 g, $6.94 \times 10^{-2}\text{ mol}$) was introduced in a round bottom flask in a glove box along
 114 with 14 mL of toluene, and heat-solubilized at 60 °C. $\text{La}(\text{BH}_4)_3(\text{THF})_3$ (35 mg,
 115 $8.67 \times 10^{-5}\text{ mol}$) was solubilized in 7 mL of toluene in the glove box before being
 116 added to the monomer solution. The reaction was conducted at 60 °C for 24 min
 117 under stirring, leading to a conversion of 51%. At the end of the reaction, the highly
 118 viscous medium was dissolved in non-anhydrous chloroform. An aliquot of the
 119 obtained solution was taken and dried under vacuum to determine the conversion by
 120 ^1H NMR in CDCl_3 . The PLA in solution in chloroform was then poured in diethyl
 121 ether. The precipitated PLA was filtered and dried under vacuum, affording purified
 122 PLA with residual monomer content of 2% ($M_n = 29,000\text{ g mol}^{-1}$, $D = 1.38$).
 123 The linear structure of the obtained PLA was confirmed by MALDI-ToF analysis.
 124 (Fig. 1b).

125 *Films Elaboration* was carried out by means of compression molding using a Dar-
 126 ragon Press. Compression molding was carried out at 200 °C for 3 min (2 min of
 127 melting without pressure and 1 min under a pressure of 50 bars), and then, the sam-
 128 ples were cooled by air. Tensile test samples were obtained from these films (about
 129 0.2 mm thick). Particularly, the dumbbell-shaped samples (28 mm of length and
 130 5 mm of width) were obtained by laser cutting using a Trotec's Speedy 400 TM
 131 Laser Cutting.

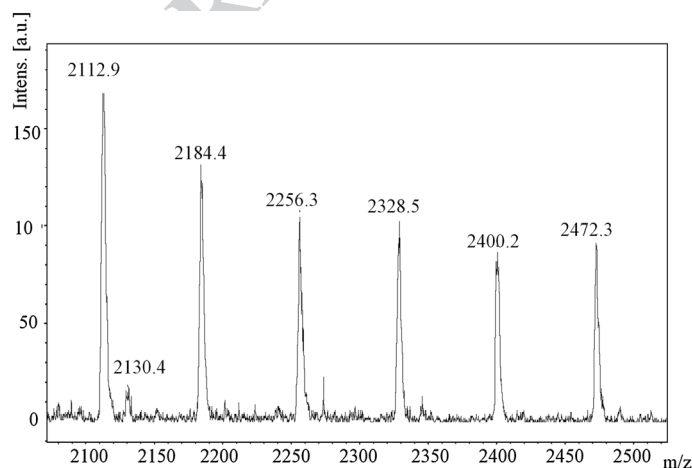


Fig. 1 MALDI-ToF spectrum of purified macrocyclic PLLA synthesized in this study

132 Characterization techniques

133 *Liquid ¹H NMR* ¹H NMR spectra of polylactides were recorded on a Bruker Avance
 134 300 MHz instrument at 300 K in CDCl₃. The chemical shifts were calibrated using
 135 the residual resonances of the solvent. The samples (about 5 to 15 mg) were dis-
 136 solved in 0.5 mL of CDCl₃ in a 5 mm diameter tube. The scan number was set to
 137 32 and the delay (D1) between each scan was set at 4 s. For the spectra relative to
 138 the chain-end analysis to confirm the cyclic or linear structure of the polymer, the
 139 number of scans of the ¹H NMR analysis was set up at 256 scans. The conversion
 140 of the reaction was determined by integration of the CH signals of both the residual
 141 monomer and the polymer at 5.05 ppm and 5.15 ppm, respectively.

142 *SEC measurements* The number-average molar masses (M_n) and dispersities
 143 ($\bar{D} = M_w/M_n$) of the polylactides were determined by size exclusion chromatogra-
 144 phy (SEC) in THF at 40 °C (1 mL/min) with a triple detection system, equipped
 145 with an Alliance Waters e2695, a multiangle light scattering detector (MALS, Wyatt
 146 Technology mini DAWN TREOS), and a refractive index detector (Waters 2414).
 147 The SEC system was equipped with three Waters Styragel (HT1, HT3 and HT4)
 148 columns.

149 The MALS method was used to determine the absolute molar masses of the
 150 cyclic PLLA. The differential refractive index (DRI) increment (dn/dc) value was
 151 determined for our macrocyclic PLA and found to be 0.0478 mL g⁻¹ in THF at
 152 40 °C [12]. The M_n values of the linear polylactide were determined according to
 153 the signal of the refractive index detector with polystyrene standards calibration and
 154 Mark-Houwink correction with coefficient 0.58. Samples were prepared by dissolv-
 155 ing the product (~10 mg) in 4 mL of THF. The solutions were then filtered with
 156 0.45 µm filters.

157 *MALDI-TOF mass spectroscopy measurements* Mass spectra were recorded by
 158 matrix-assisted laser desorption and ionization time-of-flight (MALDI-TOF) mass
 159 spectrometry using a Bruker autoflex III smartbeam mass spectrometer, equipped
 160 with the laser that produces pulses at 337 nm using dithranol as a matrix and NaI as
 161 cationizing agent. Spectra were recorded in linear mode at an accelerating potential
 162 of 20 kV. Samples were prepared by dissolving the polymer in THF at a concentra-
 163 tion of 2–5 mg mL⁻¹. A 10 µL aliquot of this solution was mixed with 20 µL of
 164 matrix solution and 10 µL of NaI solution (both at 20 mg mL⁻¹ in THF). Standards
 165 (polystyrenes of known structure, purchased from Polymer Standards Service) were
 166 used to calibrate the mass scale.

167 *DSC analysis* Thermal analyses were carried out using differential scanning calo-
 168 rimetry (DSC) (TA Instruments Q20). All DSC experiments were performed under
 169 a nitrogen atmosphere. The apparatus was calibrated thanks to an indium sample of
 170 high purity according to standard procedures. The sample weight was in the range
 171 5–15 mg, and heating and cooling rates were set at 10 °C/min.

172 Samples were first heated until 200 °C in order to erase thermal history
 173 and then cooled down to room temperature before being reheated. Thermal

characteristics were determined from the second heating. Particularly, the glass transition temperature (T_g) is taken at the half of the heat capacity jump and the melting temperature (T_m) at the maximum of the endothermic peak.

The initial degree of crystallinity has been calculated according to the following relation:

$$x_c = \frac{(\Delta H_m - \Delta H_{cc})}{\Delta H_m^0}$$

With ΔH_m , the PLA melting enthalpy determined from the endothermic peak area, ΔH_{cc} , the cold crystallization enthalpy determined from the exothermic peak, ΔH_m^0 , the standard melting enthalpy of PLA taken equal to 93 J/g [25].

Isothermal crystallization kinetics of both macrocyclic and linear polylactides were also studied for different crystallization temperatures (T_c). Samples were heated up to 200 °C then rapidly cooled down to the desired T_c using a cooling rate of 50 °C/min and held at T_c during 30 min.

Wide Angle X-ray Scattering WAXS experiments were performed using a Xeuss apparatus (Xenos, France) The Cu-K α radiation used was selected with a curved mirror monochromator. The 2D patterns were recorded on a Pilatus hybrid pixel detector (Dectris, Swiss) and the working distance, around 10 cm, was calibrated using a silver behenate sample. 2D WAXS patterns were azimuthally integrated using the Foxtrot software. Crystallinity degrees of stretched samples have been computed using the method from ref [26].

Tensile tests. Tensile tests were conducted on an Instron 4466 equipment. Two sets of conditions were used:

- tests at 25 °C with an initial strain rate of 10^{-2} s^{-1} in order to determine the Young's modulus in the glassy state.
- tests at 70 °C with an initial strain rate of 4.10^{-2} s^{-1} in order to determine the mechanical behavior of the materials in the rubbery state.

For each set of conditions and each sample type, 5 tests were carried out.

Engineering stress (σ) was calculated as the ratio $\sigma = F/S_0$ where F is the measured force and S_0 the initial cross section of the sample. Engineering strain (ϵ) is defined as the ratio between the displacement and the initial length of the sample l_0 ($\epsilon = \frac{\Delta l}{l_0}$).

The Young's modulus (E) was calculated as the slope in the linear region of the engineering stress–strain curve (i.e., between 0 and 0.1%). Finally, strain at break (σ_{break}) was taken as the engineering strain when the sample broke.

Dynamic mechanical analysis Viscoelastic properties were determined by means of DMA experiments. A RSA3 apparatus (TA Instruments, USA) was used in tensile mode. Experiments were carried out on 1-mm-thick samples elaborated using the

212 same conditions as previously described. Viscoelastic properties, namely E' and E'' ,
 213 were determined with an applied strain of 0.01% at temperatures varying from 45
 214 to 70 °C on the 0.05–50 Hz frequency range. From these tests, the mastercurves for
 215 both linear cyclic PLA were generated using the TA Orchestrator software at a refer-
 216 ence temperature $T_0 = 70$ °C.

217 Results

218 Synthesis of macrocyclic and linear PLLAs

219 In order to study the influence of the topology of the PLLA on its thermal and
 220 mechanical properties, both macrocyclic and linear polymers displaying the same
 221 molar mass were synthesized (Table 1). Macrocyclic PLLA was obtained by reac-
 222 tive extrusion polymerization of L-lactide (in bulk, in the absence of solvent) with
 223 lanthanide trisborohydride as the catalyst, according to the procedure reported in our
 224 previous study [12]. In order to get materials resistant enough to perform mechani-
 225 cal tests, the lanthanum complex $\text{La}(\text{BH}_4)_3(\text{THF})_3$ was selected as the catalyst [12],
 226 as it gave rise to the formation of macrocycles displaying the highest molar mass of
 227 30,000 g mol⁻¹. The reaction was carried out at 130 °C for 80 min, leading to 85%
 228 of conversion.

229 To ensure the purity of the obtained polymer, the residual monomer was removed **AQ1**
 230 by sublimation under vacuum in order to preserve the macrocyclic structure of
 231 PLLA. This method led to an overall residual L-Lactide content of 3%. The obtain-
 232 ing of macrocyclic PLLA was checked by ¹H NMR analysis. MALDI-ToF spectrum
 233 of the crude (Figure S4) and purified sample (Fig. 1b) displays a main population
 234 relative to macrocyclic polymer and a very minor population relative to HO-PLLA-
 235 H, arising from ring-opened macrocycles. Both MALDI-TOF spectra show distri-
 236 butions containing both even-membered and odd-membered oligomers, with peaks
 237 separated by 72 Da, indicating the occurrence of transesterification reactions (intra-
 238 molecular transesterification giving rise to cyclic PLLA). In addition, the macrocy-
 239 clic PLLA was analyzed by ¹H NMR analysis. The signal relative to the chain-end
 240 of the residual linear PLLA, HOCHMe expected at $\delta = 4.33$ ppm in CDCl₃ could be

Table 1 Macrocyclic and linear polylactides synthesized in this study

PLLA	M_n^{SEC} (g mol ⁻¹) ^c	\bar{D}^c
Macrocyclic ^a	29,490	1.27
Linear ^b	29,000	1.38

^aSynthesized by reaction extrusion with $\text{La}(\text{BH}_4)_3(\text{THF})_3$ as the catalyst. Experimental conditions: m L-LA = 20 g, $[\text{L-LA}]/[\text{La}] = 1000$; $T = 130$ °C; $t = 80$ min, L-LA non purified, 100 rpm, under nitrogen

^bSynthesized in toluene with $\text{La}(\text{BH}_4)_3(\text{THF})_3$ according to the literature procedure.¹⁷

^cDetermined by SEC (MALLS) in THF at 40 °C, $\bar{D} = M_w/M_n$

observed in the baseline of the ^1H spectrum (256 scans) of the crude polymer, but was so low that it was not integrable (Figure S1). Thus, one can conclude that the residual linear fraction in the PLLA was inferior to 1%. SEC analysis of the final polylactide confirmed a molar mass of $29\,490\text{ g mol}^{-1}$ and a dispersity of 1.27 (Figure S2).

Regarding the synthesis of the linear polylactide with a molar mass close to the one of the macrocyclic polymer, *i.e.*, about $30,000\text{ g mol}^{-1}$, a literature procedure involving the same catalyst but in the presence of solvent during the polymerization reaction was used [24]. This reaction procedure is known to afford purely linear dihydroxytelechelic polylactide, [24] whereas our recent study showed that when the same reaction was conducted in bulk conditions (in the absence of solvent), macrocyclic PLLA was obtained [12]. Thus, the polymerization of L-lactide with $\text{La}(\text{BH}_4)_3(\text{THF})_3$ as the catalyst was conducted in toluene at 60°C for 25 min, leading to 51% of conversion. The polymer was purified by being poured in diethyl ether. SEC analysis of the final polylactide confirmed a molar mass of $29,000\text{ g mol}^{-1}$ and a dispersity of 1.38 (Figure S3). MALDI-ToF analysis confirmed the linear nature of the obtained polylactide (Figure S5).

In order to measure the influence of their topology on their thermal and mechanical properties, both macrocyclic and linear PLAs were subjected to X-ray analysis, DSC analysis as well as tensile tests.

Thermal behavior

Thermal analyses were conducted by differential scanning calorimetry (DSC) on both macrocyclic and linear PLA samples (Fig. 2). The values of the different thermal characteristics are summarized in Table 2. Thermal characteristics of macrocyclic and linear PLAs are measured on second heat.

As shown by the DSC traces depicted in Fig. 2, upon cooling, the macrocyclic PLA exhibits a small crystallization peak at 93°C (marked by a *) while the linear PLA displays a much more intense one at 98°C . This indicates that macrocyclic PLA has a slower crystallization kinetic, which may suggest that the macrocyclic structure restrains the molecular mobility.

In the case of the macrocyclic PLA, a glass transition occurs at around 56°C during the second heating, followed by an exotherm around 106°C which corresponds to the cold crystallization process. One can also notice the presence of a double

Table 2 Thermal characteristics of macrocyclic and linear PLAs measured on second heat

	Macrocyclic PLA	Linear PLA
T_g ($^\circ\text{C}$)	56 ± 1	53 ± 1
T_{cc} ($^\circ\text{C}$)	106 ± 2	96 ± 2
ΔH_{cc} (J/g)	35 ± 3	4.4 ± 0.5
T_f ($^\circ\text{C}$)	165 ± 2	171 ± 2
ΔH_m (J/g)	42 ± 1	50 ± 1
Initial crystallinity (%)	7 ± 5	49 ± 5

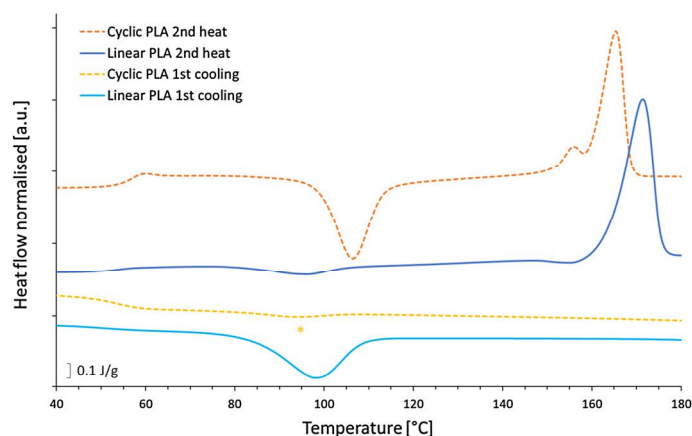


Fig. 2 DSC of macrocyclic and linear PLAs; cooling from the melt at 10 °C/min and subsequent heating at 10 °C/min (endo up)

melting peak at 156 & 165 °C. This phenomenon may be explained by two assumptions: either the existence of two different PLA crystalline structures, displaying different T_f (which was unvalidated by X-ray, see below), or a recrystallization melting phenomenon [27, 28], i.e., there is the fusion of a certain amount of the original crystals (at the beginning of the melting), immediately followed by recrystallization into more perfect crystals and final melting of these more perfect crystals.

Regarding the linear PLA, the glass transition is observed at 53 °C, i.e., at a slightly lower temperature than for macrocyclic one, followed by a very small cold crystallization peak at 96 °C and a melting peak at 171 °C.

A 4 °C higher T_g for cyclic PLA as compared to linear PLA has been also reported by Zaldua et al. [19]. The authors explain this difference by the fact that cyclic PLA chains have no chain-ends. As these chain-ends are highly mobile and generate free volume, they are assumed to be responsible of the lower T_g of linear PLA. The latter point cannot alone explain the difference observed regarding the glass transition temperatures. Indeed, the same difference of T_g is observed in the present study and in the one of Zaldua et al. while the chain ends number for linear PLA is about 3 times lower in our case. Consequently, we rather assume that the higher T_g for cyclic PLA depicts a higher rigidity of the chains and/or differences into the macromolecular network due to the cyclic macrostructure rather than to a key role of the chain-ends.

In addition, the higher melting temperature of linear PLA tends to show that thicker and/or more perfect crystals are formed in this material. Regarding the melting peak areas, results show that crystal content induced during the cooling and subsequent heating steps is higher for linear PLA (53% of crystallinity vs 45% for the macrocyclic one), suggesting its stronger ability to crystallize.

In summary, in addition to a slightly higher T_g , macrocyclic PLA seems to have a slower crystallization kinetic than its linear analog, as revealed by the fairly lower amplitude of the crystallization process upon cooling from the melt. Indeed, the

crystallinity degree after cooling at 10 °C/min is about 49% for linear PLA, while it is only 7% for the macrocyclic one. This behavior differs from the one reported in the case of cyclic PLA exhibiting much lower M_n [19], where they observed that cyclic PLA has a faster crystallization kinetics than the linear counterpart.

In order to confirm that macrocyclic PLA has a lower ability to crystallize, a study of the crystallization kinetics was carried out on the two polylactides samples (Fig. 3). Particularly, isothermal crystallizations from the melt state were performed at temperatures varying from 80 to 140 °C with 10 °C steps.

The slower crystallization kinetics of macrocyclic PLA is confirmed by the behaviors observed for the crystallizations ranging from 90 °C to 120 °C where the exotherm related to the crystallization of macrocyclic PLA is systematically broader and starts at longer times. Indeed the crystallization time never exceeds 5 min in the case of linear PLA, while the minimum crystallization time of macrocyclic PLA is 10 min (isothermal at 110 °C).

In addition, no crystallization is observed for both linear and macrocyclic PLAs at $T_c = 140$ °C during the experiment time. At this temperature, crystallization is mainly governed by nucleation aspects (as crystal growth is favored at high temperature) and the higher nucleation ability of cyclic PLA reported by Zaldua et al. [19] does not seem to be observed here. This can be explained by the fact that, as previously mentioned, the molar mass of their material is close to the mass between entanglements of PLA. Consequently, the higher ability to crystallize cyclic PLA may arise from the fact that the chains are very little entangled. In our case, both macrocyclic and linear PLA chains are entangled and as discussed below it could be assumed that the entanglements in the case of cyclic macromolecules are more restrictive from a mobility point of view than the entanglements in the case of linear macromolecules.

In opposition, for $T_c = 80$ °C, an exothermic peak is clearly observed for the linear PLA. By contrast, no crystallization peak is evidenced for the macrocyclic PLA. At

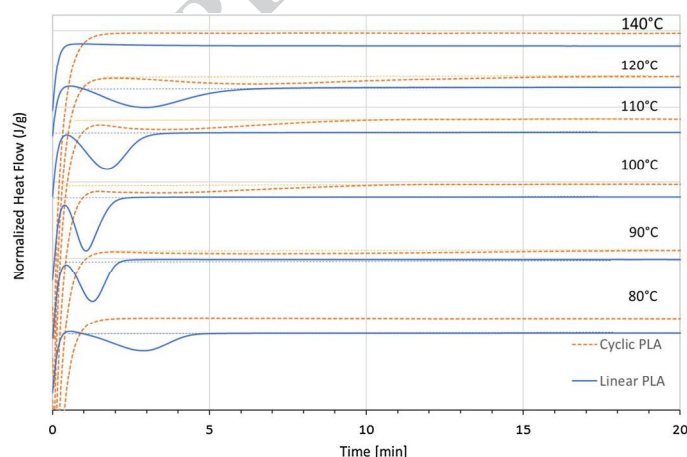


Fig. 3 Crystallization kinetics at different isothermal temperatures of macrocyclic and linear PLA (end up)

low temperature, it is nucleation which is favored, then crystallization is mainly governed by growth rates aspects. Considering that the two materials have similar molar mass, this difference thus necessarily arises from the different molecular architectures of the PLA and it can be thus conclude that the macrocyclic microstructure involves a slower crystal growth rate due to lower molecular mobility.

Several works have been reported on the crystallization of cyclic and linear polymers. A review of these studies points out that up to now, no unique behavior can be observed. Besides, two opposite trends have been found: the crystallization is slower for cyclic PTHF and PE than for linear analogs (transport and secondary nucleation require higher free energies in cyclic polymers), but faster for cyclic poly(oxyethylene) (POE) and PCL (faster diffusion of cyclic molecules) than for linear analogs [29]. Thus in our case, this behavior could be due to a better mobility of the linear chains compared to the macrocyclic ones, which would allow them to arrange more easily to form the crystal lattice.

Comparing these two studies, we could conclude that linear PLA has a higher ability to crystallize, particularly at low temperatures. Moreover, the macrocyclic structure involves the formation of thinner and/or less perfect crystals.

Structural characterization

Macrocyclic and linear PLAs that have undergone an isotherm at 120 °C were analyzed by means of wide-angle X-ray scattering (WAXS) after recrystallization (Fig. 4). Results indicate that both polymers are semi-crystalline, and the position of the diffraction peaks (13.6°, 14.6°, 16.6° and 22.3°) shows that they crystallize into the α phase [30] in agreement with previously reported results [19].

The crystallinity ratios calculated by XRD are in line with the DSC results, i.e., 50% for the macrocyclic PLA and 59% for the linear one, which confirms that the macrocyclic polymer displays a lower crystallinity degree than its linear analog.

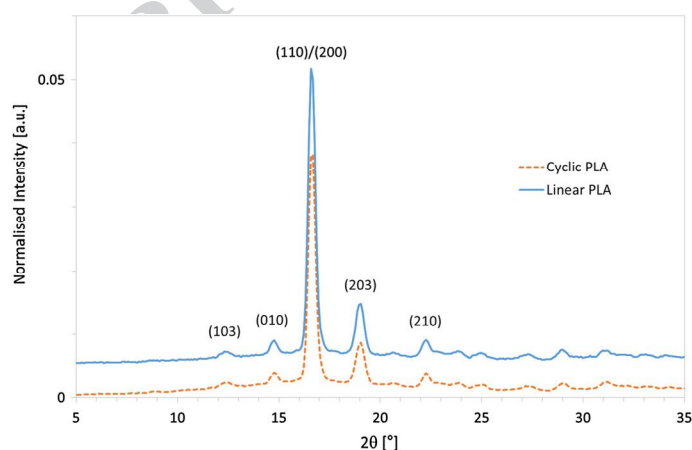


Fig. 4 Diffraction pattern of the PLAs film annealed

Table 3 Summary of tensile tests results at 25 °C

	E (MPa)	σ_{break} (MPa)	ϵ_{break} (%)
Macrocytic PLA	2510 ± 98	32 ± 2	1 ± 1
Linear PLA	2408 ± 278	36 ± 7	1.5 ± 1

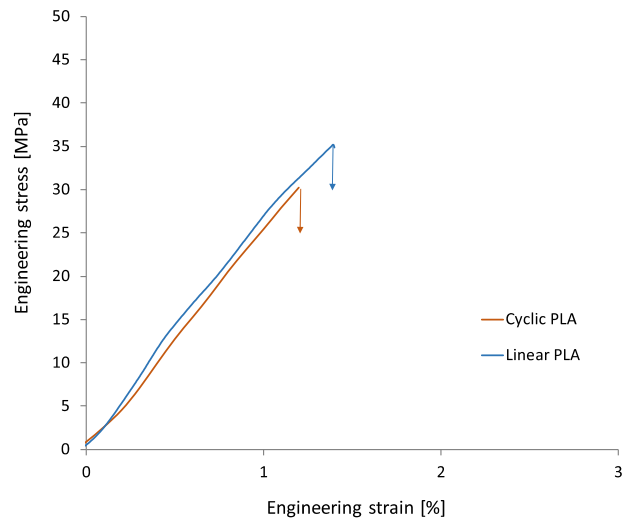


Fig. 5 Engineering stress–strain curves at 25 °C and $\dot{\epsilon} = 10^{-2} \text{ s}^{-1}$

Mechanical study of macrocytic and linear PLAs

Tensile tests were performed on amorphous films obtained by compression molding. A set of experiments were carried out at 25 °C in order to determine the end-to-use properties of the materials. Mechanical properties are reported in Table 3.

At 25 °C (Fig. 5), both materials exhibit a brittle behavior with no sign of plastic deformation. In addition, both materials have roughly the same Young's modulus, around 2.5 GPa, characteristic of an amorphous polymer into its glassy state. Consequently, no main difference can be observed during cold-drawing.

Mechanical properties were also studied in the rubbery state (Fig. 6). The drawing temperature has been chosen so as to be between T_g and T_{cc} , i.e., at sufficiently high temperature to obtain materials in their rubbery state and sufficiently low temperature to prevent any thermally induced crystallization phenomenon.

The mechanical behavior is roughly the same whatever the PLA type and characteristic of an initially amorphous sample drawn in its rubbery state (e.g., PET). Besides, after a viscoelastic deformation stage at low strains, plastic deformation occurs at a similar strain value. Then, for larger deformations, a strain-hardening phenomenon is observed in both cases. The main differences between the two materials are that strain-hardening starts at lower strains for macrocytic PLA

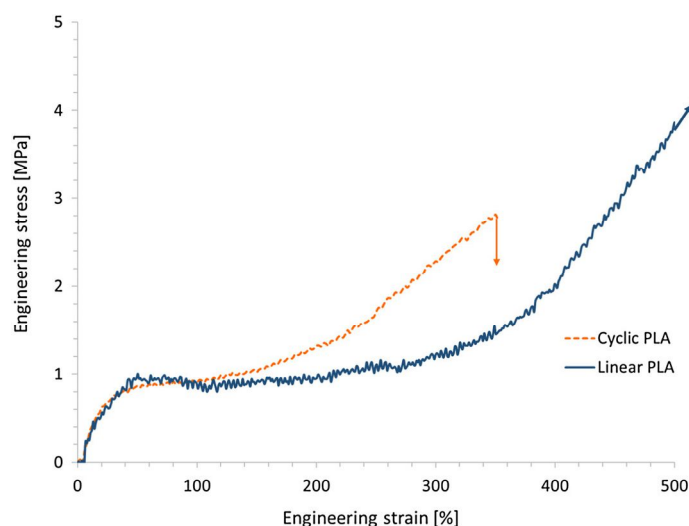


Fig. 6 Engineering stress–strain curves at 70 °C and $\dot{\epsilon} = 10^{-2} \text{ s}^{-1}$

(i.e., 200% for macrocyclic PLA vs 350% for linear PLA). In the case of PLA, strain-hardening is related to the occurrence of a strain-induced crystallization, the beginning of crystallization being governed by the achievement of a critical macromolecular orientation degree. Consequently, it can be assumed that macrocyclic PLA has a better ability to macromolecular orientation upon stretching. Finally, it is also observed that the linear PLA can undergo a very large deformation at break, i.e., > 500% while the one of cyclic PLAs is lower, around 400%.

In order to confirm the occurrence of strain-induced crystallization upon stretching, and in order to assess the influence of the topology on the strain-induced structure, post-mortem WAXS analyses were also performed on drawn samples and comparison of patterns and diffractograms before and after the tensile tests are presented in Figs. 7 and 8. The values of the crystallinity rate calculated by XRD are summarized in Table 4.

Before stretching both linear and macrocyclic PLAs are fully amorphous, as shown in the 2D WAXS images (Fig. 7) and the crystallinity rate (Table 3). After stretching (300% of strain for macrocyclic PLA vs 430% for the linear one), the integrated intensity profiles (Fig. 8) clearly show the presence of crystals into both materials confirming that the occurrence of strain-induced crystallization is at the

Table 4 Crystallinity degree calculated by XRD

	Macrocyclic PLA BT	Macrocyclic PLA AT70	Linear PLA BT	Linear PLA AT70
Crystallinity (%)	0	35 ± 5	0	40 ± 5

BT before traction; AT70: After Traction at 70 °C

Author Proof

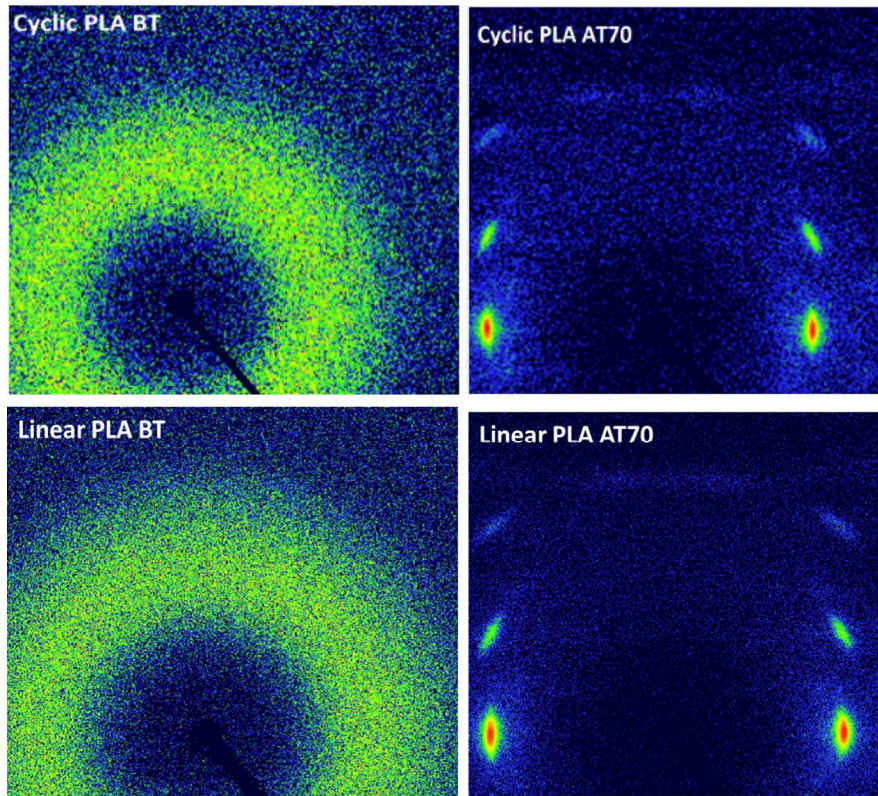


Fig. 7 Diffraction patterns of PLAs before (BT) and after (AT70) tensile tests at 70 °C (the stretching axis is vertical)

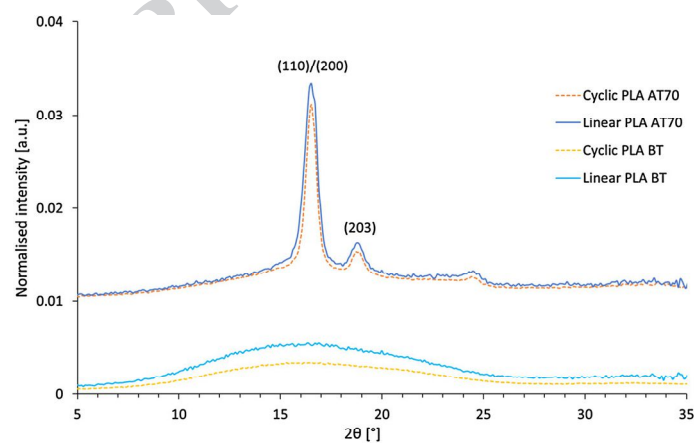


Fig. 8 Diffraction pattern of PLAs before (BT) and after (AT70) tensile tests at 70 °C

origin of the strain-hardening stage observed on the stress–strain curves. The earlier occurrence of strain-induced crystallization for macrocyclic PLA is probably ascribed to a faster increase in the macromolecular orientation upon stretching, as compared to linear PLA.

Moreover, the position of the diffraction peaks shows that it is the α' phase (Fig. 8) which is involved in both cases [31]. Finally, we also note that the crystallinity rates of macrocyclic PLA (35%) is slightly lower than the one of linear PLAs (40%) (Table 3).

Discussion: Entanglement in cyclic and linear structures

The examination of the mechanical behavior in the rubbery state, and in particular the earlier occurrence of the strain-induced crystallization process in the case of macrocyclic PLA, may suggests that the entanglement network of the macrocyclic PLA is more constrained than the one of the linear one. Indeed the occurrence of strain-induced crystallization in PLA could be linked with an achievement of a critical orientation degree of the macromolecules [32]. Consequently, it appears that in macrocyclic PLA, the macromolecules orient faster upon stretching than in linear PLA which tends to show that macrocycles have a slower disentanglement kinetics than the linear chains which favors macromolecular orientation upon stretching explaining the difference in the mechanical behavior observed.

The examination of the viscoelastic properties, especially in the rubbery domain, is known to be a good probe of the macromolecular architecture. Notably, the value of the storage modulus in this region could be directly related to the mass between the entanglements of the polymer according to the following equation:

$$M_e = \frac{\rho RT}{G_N^0}$$

with G_N^0 being the value of the storage modulus G' measured in plateau modulus (at the minimum of the loss modulus G''), ρ the density of the material at the considered temperature, R the universal gas constant and T the considered temperature in K. In our study, viscoelastic properties were determined in the tensile mode, however, as G' and E' are proportional the previous equation can also be applied. Figure 9 depicts the mastercurves obtained for both cyclic and linear PLAs at the reference temperature $T_0 = 70^\circ\text{C}$.

The value of M_e , could be assessed by the determination of E' in the low frequency region, where the materials are in the rubbery state. Experiments were repeated three times for each material, and the analyses revealed that no differences could be observed regarding the plateau modulus, around 4 MPa, for both macrocyclic and linear PLAs. Consequently, the macrocyclic structure does not infer on the mass between the entanglements of PLA. The only slight difference which can be evidenced from these experiments is that the crossover point between E' and E'' occurs at a slightly higher frequency ω_c for linear PLA. $1/\omega_c$ could be related to a characteristic relaxation of the material [33] and thus, even if both times are of the

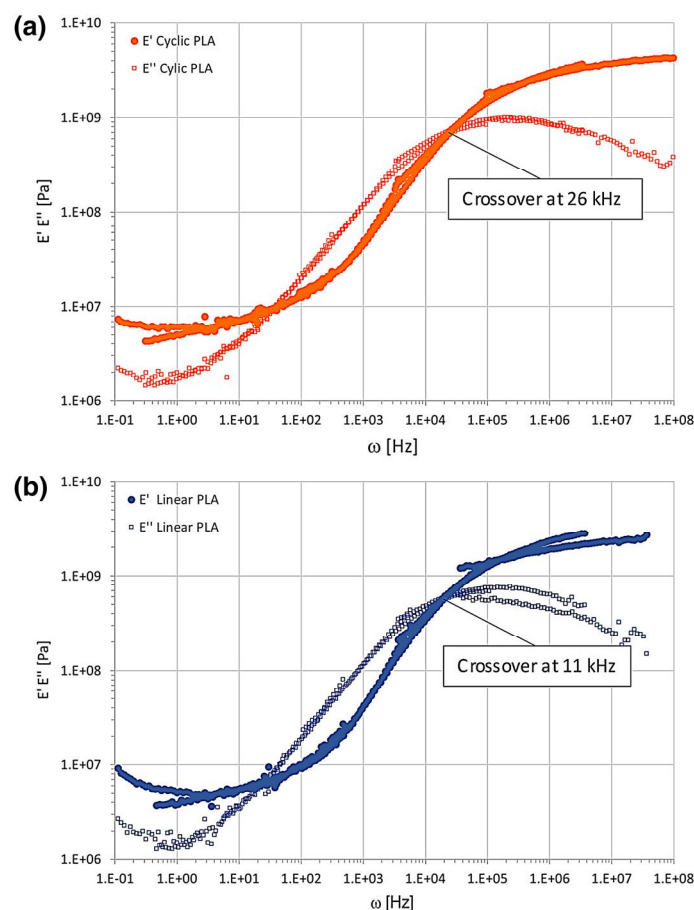


Fig. 9 Storage modulus (E') and loss modulus (E'') as a function of frequency at $T_0 = 70^\circ\text{C}$ for **a** macrocyclic PLA and **b** linear PLA

433 same order of magnitude, the relaxation time of linear PLA is slightly lower than the
434 one of its macrocyclic analog.

435 The observation of a rubbery plateau for PLA seems to be in contradiction with
436 the results obtained by Doi et al. in the case of polystyrene (PS) [34]. Indeed in their
437 study where they analyze the viscoelastic behavior of ring PS with various molecu-
438 lar weights, authors never observe a rubbery plateau. However, they nevertheless
439 observe for high molecular weight PS, a deviation to the standard behavior (i.e.,
440 Rouse like model). Authors attribute this deviation to the formation of intermolecu-
441 lar interactions such as ring penetrations. The fact that a rubbery plateau is observed
442 in our case for macrocyclic PLA also shows that (i) the macrocycles can also entan-
443 gle themselves, and (ii) that the entanglement network is more stable in PLA than
444 in PS. This higher stability for PLA should be explained by the differences of Me
445 between PS and PLA. Indeed, considering that PLA and PS exhibit similar values

regarding the chain rigidity [35–37], the M_e of PLA is about 4–5 times lower than the one of PS. Consequently, the entanglement network formed by the PLA macrocycle is probably more constrained, i.e., the macromolecules have less mobility.

As a result of this work, and in the same way than what was shown by Doi et al. for PS [34], the macromolecular network understanding seems to be a key point to explain the behavior differences between cyclic polymers and their linear analogues. Besides, it appears that the fact that the molar mass of the material is below or above M_c significantly changes the material behavior. On the one hand, when M_n is below M_c , cyclic PLA displays a faster macromolecular dynamics involving besides a faster crystallization kinetics than its linear counterpart. On the other hand, when the materials are entangled (i.e., when M_n is above M_c as in this study), the crystallization kinetics is slower for macrocyclic PLA and this material has a faster macromolecular orientation rate upon stretching.

The macromolecular network and the concept of entanglement have been deeply studied in the case of linear polymers and are now well understood as depicted in Fig. 10a. On the other hand, entanglements in cyclic polymers as well as the macromolecular organization in the amorphous bulk remain poorly addressed. An attempt of structural representation is schematized in Fig. 10b, and, as can be seen, interpenetration of macrocycles can lead to locally completely locked structures contrary to the case of linear polymer where the chains can disentangle more easily due to fact that they do not form a closed structure and are consequently more labile. Similar locked structures have been also proposed by Submarian et al. in their modeling study of DNA [38]. Still using a numerical approach, threading, i.e., interpenetration, between large cycles has also been proposed by Lee et al. [39] as well as Tsalikis et al. [40].

This representation also allows to understand the lower mobility of macrocyclic chains. Indeed, it clearly appears that the interpenetration of macrocycles could lead to a more constrained network with less mobility degrees. This explains the slower crystallization kinetics observed for macrocyclic PLA. In addition, the presence of these locally locked structures formed by the interpenetration of two macrocycles could be at the origin of the faster macromolecular orientation observed during stretching in the rubbery state as previously discussed. Indeed, due to these constraints the relaxation time of macrocyclic PLA chains is higher than that of linear PLA (see DMA results). Consequently, upon stretching, the macrocyclic PLA chains relax less than the ones of linear PLA and thus orient themselves faster involving an earlier occurrence of strain-induced crystallization.

Conclusion

This study aimed at comparing the behavior between macrocyclic and linear polylactides displaying identical molar masses, allowing to highlight the influence of the polymer topology on its structure and properties. Regarding thermal properties, the glass transition temperature of the macrocyclic PLA is slightly higher than that of the linear one as expected (56 vs. 53 °C) [13–15], while its

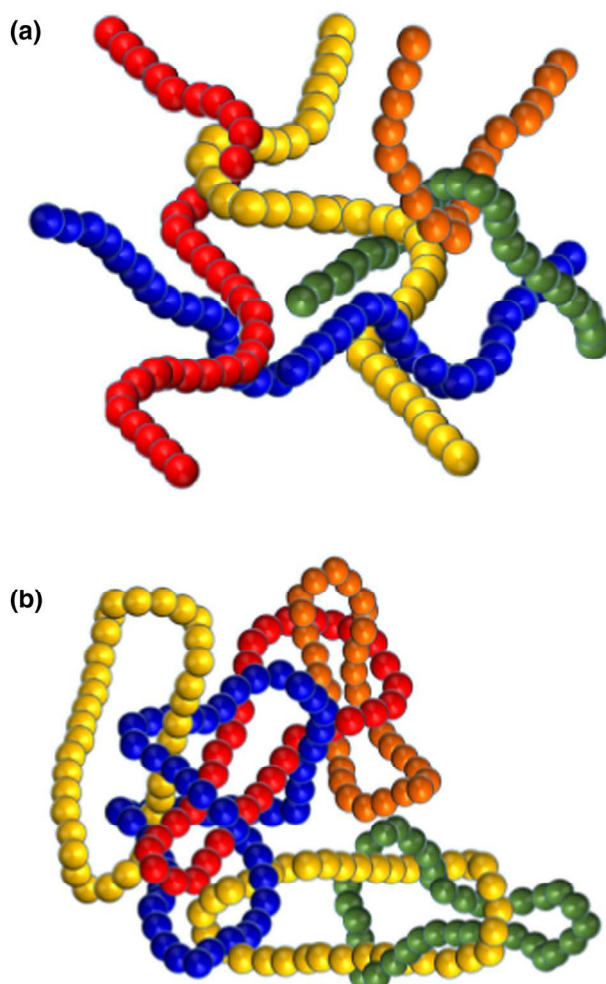


Fig. 10 Schematic representation of the macromolecular networks in the cases of **a** a linear polymer and **b** a cyclic polymer

melting point is lower (165 vs. 171 °C) indicating that the macrocyclic architecture induces the formation of smaller and/or more defective crystals.

Moreover, the crystallization kinetics of PLA is strongly influenced by its topology. Indeed, macrocyclic PLA has a lower crystallinity, *i.e.*, 50% vs 59% for the linear one (XRD) but especially has a slower crystallization kinetics which is ascribed to the fact that the macrocyclic structure restricts the molecular mobility. Tensile tests conducted at 70 °C showed that linear PLA had a much higher deformation capacity than its macrocyclic analog. This is attributed to the more constrained macromolecular network of the macrocyclic PLA and could have some implications regarding its processing. Finally, regarding the strain-induced

structure under tensile tests at 70 °C and the mechanical properties at room temperature, no significant difference between the two materials was evidenced.

Author Proof

Acknowledgements The authors would like to thank Aurélie Malfait for SEC analysis, Dr François Stoffelbach for MALDI-ToF analysis, CNRS and Région Hauts de France for fundings. The project ARCHI-CM, Chevreul Institute (FR 2638), Ministère de l'Enseignement Supérieur et de la Recherche, Région Nord-Pas de Calais and European Regional Development Fund (FEDER) are acknowledged for supporting and funding the SAXS-WAXS laboratory.

References

- Auras R, Lim L-T, Selke SEM, Tsuji H (2010) Poly(Lactic Acid): Synthesis, structures, properties, processing, and applications. Wiley, Hoboken
- Jamshidian M, Tehrani EA, Imran M, Jacquot M, Desobry S (2010) Poly-lactic acid: production, applications, nanocomposites, and release studies. *Compr Rev Food Sci F* 9:552–571. <https://doi.org/10.1111/j.1541-4337.2010.00126.x>
- Slomkowski S, Penczek S, Duda A (2014) Polylactides: an overview. *Polym Adv Tech* 25(5):436–447. <https://doi.org/10.1002/pat.3281>
- Pawar RP, Tekale SU, Shisodia SU, Totre JT, Domb AJ (2014) Biomedical applications of poly(lactic acid). *Recent Pat Regen Med* 4:40–51. <https://doi.org/10.2174/2210296504666140402235024>
- Krishnan S, Pandey P, Mohanty S, Nayak SK (2016) Toughening of polylactic acid: an overview of research progress. *Polym Plast Technol Eng* 55(15):1623–1652. <https://doi.org/10.1080/03602559.2015.1098698>
- Murariu M, Dubois P (2016) PLA composites: from production to properties. *Adv Drug Deliv Rev* 107:17–46. <https://doi.org/10.1016/j.addr.2016.04.003>
- Dechy-Cabaret O, Martin-Vaca B, Bourissou D (2004) Controlled ring-opening polymerization of lactide and glycolide. *Chem Rev* 104(12):6147–6176. <https://doi.org/10.1021/cr040002s>
- Jérôme C, Lecomte P (2008) Recent advances in the synthesis of aliphatic polyesters by ring-opening polymerization. *Adv Drug Deliv Rev* 60(9):1056–1076. <https://doi.org/10.1016/j.addr.2008.02.008>
- Dagorne S, Normand M, Kirillov E, Carpentier J-F (2013) Gallium and indium complexes for ring-opening polymerization of cyclic ethers, esters and carbonates. *Coord Chem Rev* 257(11–12):1869–1886. <https://doi.org/10.1016/j.ccr.2013.02.012>
- Carpentier J-F (2010) Discrete metal catalysts for stereoselective ring-opening polymerization of chiral racemic β -Lactones. *Macromol Rapid Commun* 31(19):1696–1705. <https://doi.org/10.1002/marc.201000114>
- Hakkarainen M (2002) Aliphatic polyesters: abiotic and biotic degradation and degradation products. In: *Degradable aliphatic polyesters*. Adv. Polym. Sci., vol 157. Springer, Berlin, pp 113–138
- Bonnet F, Stoffelbach F, Fontaine G, Bourbigot S (2015) Continuous cyclo-polymerisation of L-lactide by reactive extrusion using atoxic metal-based catalysts: easy access to well-defined polylactide macrocycles. *RSC Adv* 5(40):31303–31310. <https://doi.org/10.1039/C4RA16634E>
- Roovers J (2002) Chapter 10: organic cyclic polymers. In: Semlyen JA (ed) *Cyclic polymers*, 2nd edn. Kluwer, Dordrecht, pp 347–383
- Kricheldorf HR (2010) Cyclic polymers: Synthetic strategies and physical properties. *J Polym Sci A Polym Chem* 48(2):251–284. <https://doi.org/10.1002/pola.23755>
- Hoskins JN, Grayson SM (2009) Synthesis and Degradation Behavior of Cyclic Poly(ϵ -caprolactone). *Macromolecules* 42(17):6406–6413. <https://doi.org/10.1021/ma9011076>
- Nasongkla N, Chen B, Macaraeg N, Fox ME, Fréchet JMJ, Szoka FC (2009) Dependence of Pharmacokinetics and Biodistribution on Polymer Architecture: Effect of Cyclic versus Linear Polymers. *J Am Chem Soc* 131(11):3842–3843. <https://doi.org/10.1021/ja900062u>
- Chen B, Jerger K, Fréchet JM, Szoka FC (2009) The influence of polymer topology on pharmacokinetics: differences between cyclic and linear PEGylated poly(acrylic acid) comb polymers. *J Control Release* 140(3):203–209. <https://doi.org/10.1016/j.jconrel.2009.05.021>

- 549 18. Chisholm MH, Gallucci JC, Yin H (2006) Cyclic esters and cyclodepsipeptides derived from lac-
550 tidate and 2,5-morpholinediones. *Proc Natl Acad Sci U S A* 103(42):15315–15320. <https://doi.org/10.1073/pnas.0602662103>
- 551 19. Zaldua N, Liénard R, Josse T, Zubitur M, Mugica A, Iturrospe A, Arbe A, De Winter J, Coulembier
552 O, Müller AJ (2018) Influence of chain topology (cyclic versus linear) on the nucleation and isother-
553 mal crystallization of poly(l-lactide) and poly(d-lactide). *Macromolecules* 51(5):1718–1732. <https://doi.org/10.1021/acs.macromol.7b02638>
- 554 20. Stoclet G, Lefebvre JM, Séguéla R, Vanmansart C (2014) In-situ SAXS study of the plastic
555 deformation behavior of polylactide upon cold-drawing. *Polymer* 55(7):1817–1828. <https://doi.org/10.1016/j.polymer.2014.02.010>
- 556 21. Dorgan JR, Williams JS, Lewis DN (1999) Melt rheology of poly(lactic acid): Entanglement and
557 chain architecture effects. *J Rheol* 43(5):1141–1155. <https://doi.org/10.1122/1.551041>
- 558 22. Cooper-White JJ, Mackay ME (1999) Rheological properties of poly(lactides) **AQ2**
559 effect of molecular weight and temperature on the viscoelasticity of poly(l-lac-
560 tic acid). *J Polym Sci Part B Polym Phys* 37(15):1803–1814. doi:10.1002/
561 (SICI)1099-0488(19990801)37:15<1803:AID-POLB5>3.0.CO;2-M
- 562 23. Cendrowski-Guillaume SM, Le Gland G, Nierlich M, Ephritikhine M (2000) Lanthanide borohy-
563 drides as precursors to organometallic compounds. Mono(cyclooctatetraenyl) Neodymium Com-
564 plexes. *Organometallics* 19(26):5654–5660. <https://doi.org/10.1021/om000558f>
- 565 24. Nakayama Y, Sasaki K, Watabane N (2009) Ring-opening polymerization of six-membered cyclic
566 esters catalyzed by tetrahydroborate complexes of rare earth metals. *Polymer* 50(20):4788–4793.
567 <https://doi.org/10.1016/j.polymer.2009.08.024>
- 568 25. Fischer EW, Sterzel HJ, Wegner G (1973) Investigation of the structure of solution grown crystals of
569 lactide copolymers by means of chemical reactions. *Kolloid-Z.u.Z. Polymere* 251(1):980–990
- 570 26. Stoclet G, Seguela R, Lefebvre JM, Elkoun S, Vanmansart C (2010) Strain-induced molecular
571 ordering in polylactide upon uniaxial stretching. *Macromolecules* 43(3):1488–1498. <https://doi.org/10.1021/ma9024366>
- 572 27. Yasuniwa M, Tsubakihara S, Sugimoto Y, Nakafuku C (2004) Thermal analysis of the double-
573 melting behavior of poly(L-lactic acid). *J Polym Sci Part B Polym Phys* 42(1):25–32. <https://doi.org/10.1002/polb.10674>
- 574 28. Di Lorenzo ML (2006) Calorimetric analysis of the multiple melting behavior of poly(L-lactic
575 acid). *J Appl Polym Sci* 100(4):3145–3151. <https://doi.org/10.1002/app.23136>
- 576 29. Pérez-Camargo RA, Mugica A, Zubitur M, Müller AJ (2017) Crystallization of cyclic polymers. In:
577 Auriemma F, Alfonso GC, de Rosa C (eds) *Polymer Crystallization I. Advances in polymer science*,
578 vol 276. Springer, Cham, pp 93–132
- 579 30. Rahman N, Kawai T, Matsuba G, Nishida K, Kanaya T, Watanabe H, Okamoto H, Kato M, Usuki
580 A, Matsuda M, Nakajima K, Honma N (2009) Effect of polylactide stereocomplex on the crystal-
581 lization behavior of poly(l-lactic acid). *Macromolecules* 42(13):4739–4745. <https://doi.org/10.1021/ma900004d>
- 582 31. Zhang J, Tashiro K, Tsuji H, Domb AJ (2008) Disorder-to-order phase transition and multiple melt-
583 ing behavior of poly(L-lactide) investigated by simultaneous measurements of WAXD and DSC.
584 *Macromolecules* 41(4):1352–1357. <https://doi.org/10.1021/ma0706071>
- 585 32. Stoclet G, Seguela R, Lefebvre JM, Rochas C (2010) New insights on the strain-induced mesophase
586 of poly(d, l-lactide): In situ WAXS and DSC study of the thermo-mechanical stability. *Macromol-
587 ecules* 43(17):7228–7237. <https://doi.org/10.1021/ma101430c>
- 588 33. Roland CM, Archer LA, Mott PH, Sanchez-Reyes J (2004) Determining rouse relaxation
589 times from the dynamic modulus of entangled polymers. *J Rheol* 48(2):395–403. <https://doi.org/10.1122/1.1645516>
- 590 34. Doi Y, Matsubara K, Ohta Y, Nakano T, Kawaguchi D, Takahashi Y, Kawaguchi D, Takahashi Y,
591 Takano A, Matsushita Y (2015) Melt rheology of ring polystyrenes with ultrahigh purity. *Macro-
592 molecules* 48(9):3140–3147. <https://doi.org/10.1021/acs.macromol.5b00076>
- 593 35. Wu S (1992) Predicting chain conformation and entanglement of polymers from chemical structure.
594 *Polym Eng Sci* 32(12):823–830. <https://doi.org/10.1002/pen.760321209>
- 595 36. Joziassé CAP, Veenstra H, Grijpma DW, Pennings AJ (1996) On the chain stiffness of poly(lactide)
596 s. *Macromol Chem Phys* 197(7):2219–2229. <https://doi.org/10.1002/macp.1996.021970713>
- 597 37. Grijpma DW, Penning JP, Pennings AJ (1994) Chain entanglement, mechanical properties and
598 drawability of poly(lactide). *Colloid Polym Sci* 272(9):1068–1081. <https://doi.org/10.1007/BF00652375>

- 607 38. Subramanian G, Shanbhag S (2008) Conformational properties of blends of cyclic and linear poly-
608 mer melts. Phys Rev E Stat Nonlinear Soft Matter Phys. <https://doi.org/10.1103/PhysRevE.77.011801>
609 1
- 610 39. Lee E, Kim S, Jung YJ (2015) Slowing down of ring polymer diffusion caused by inter-ring thread-
611 ing. Macromol Rapid Commun 36(11):1115–1121. <https://doi.org/10.1002/marc.201400713>
- 612 40. Tsalikis DG, Mavrantzas VG (2014) Threading of ring poly(ethylene oxide) molecules by linear
613 chains in the melt. ACS Macro Lett 3(8):763–766. <https://doi.org/10.1021/mz5002096>

614 **Publisher's Note** Springer Nature remains neutral with regard to jurisdictional claims in published
615 maps and institutional affiliations.
616